Semiconductor Physics, Quantum Electronics & Optoelectronics, 2016. V. 19, N 2. P. 129-138.
doi: 10.15407/spqeo19.02.129

PACS 07.57.Kp, 73.40.-c, 85.30.Tv

Performance limits of terahertz zero biased rectifying detectors for direct detection

A.G. Golenkov, F.F. Sizov
V. Lashkaryov Institute of Semiconductor Physics, NAS of Ukraine
41, prospect Nauky, 03680 Kyiv, Ukraine; e-mail: sizov@isp.kiev.ua

Abstract. Performance limits of uncooled unbiased field effect transistors (FETs) and Schottky-barrier diodes (SBDs) as direct detection rectifying terahertz (THz) detectors operating in the broadband regime have been considered in this paper. Some basic extrinsic parasitics and detector-antenna impedance matching were taken into account. It has been concluded that, in dependence on radiation frequency, detector and antenna parameters, the ultimate optical responsivity ($\Re_{opt}$) and optical noise equivalent power (NEP_{opt}) of FETs in the broadband detection regime can achieve $\Re_{opt}$ ~ 23 kV/W and $NEP_{opt} \sim 1\cdot10^{-12}$ W/Hz$^{1/2}$, respectively. At low radiation frequency ν in the THz spectral region the NEP_{opt} of SBD detectors can be better by a factor of ~1.75 as compared to that of Si MOSFETs (metal oxide semiconductor FETs) and GaAlN/GaN HFETs (heterojunction FETs) with comparable device impedances.

Keywords: rectifying uncooled terahertz detector, NEP, FET, GaAlN/GaN heterojunction FET, SBD.

Manuscript received 18.01.16; revised version received 12.04.16; accepted for publication 08.06.16; published online 06.07.16.

1. Introduction

THz technologies (ν ~ 0.1 to 10 THz) utilizing direct detection detectors have attractive interest due to potential applications in relatively high resolution imaging, spectroscopy, medical diagnostics, biology and pharmacology, as well as security and quality-control applications (see, *e.g.* [1]). THz radiation disposed between microwaves and light shares their characteristics, which leads to composing of electronics and photonics, that's why defining application domains and advantages over other radiation frequency regions. Capability of solid-state electronics at THz frequencies is limited, since the power and efficiency of electronic microwave devices related with signal amplification, decrease or are unrealizable in the THz frequency range. It does not concern FET or SBD THz detectors under consideration as the principles of their operation in detection of THz radiation are conditioned by rectification processes at the source/drain-channel pads (FETs) or junctions (SBDs).

For many applications at ground Earth conditions, THz sources should be powerful enough to overcome an extreme THz radiation attenuation even at short distances and should be small enough to be effectively used in mobile THz systems. Still the shortage of compact and powerful terahertz sources exists [2], which restricts, *e.g.*, the active imaging THz system applications.

Along with the sources, the important components of THz technology systems are uncooled and compact detectors that should be used at Earth conditions when dense atmosphere strongly absorbs, refracts, and scatters the THz signals. These detectors are required for contemporary systems to be implemented as integrated arrays to approach the real time performance in, *e.g.*, active direct detection cost effective imaging systems.

Silicon MOSFET, III-V HFET and III-V SBD rectification detectors now are among the promising uncooled THz/sub-THz direct detection detectors to be used in linear or matrix arrays. Uncooled SBD single detectors, as compared to other ones (*e.g.*, Golay cell, pyroelectric, bolometer, FET, superlattice detectors, *etc.*), at the moment seem to be the most sensitive within the low-frequency THz range (ν<~300 GHz) where their NEP can reach NEP ~$10^{-11}\ldots4\cdot10^{-13}$ W/Hz$^{1/2}$ (see [3-6], for Refs. see also [7]) in dependence on the radiation frequency range, antenna and detector impedances, antenna-detector matching, *etc.* They have long been used since 1940s for microwave detection and mixing because of their relatively high sensitivity, speed and ability to operate at ambient or cryogenic temperatures.

The study of FETs as THz detectors was initiated by the Dyakonov–Shur [8] theory developed for HFETs in hydrodynamic approximation (drift current, strong inversion region) though images by small number of GaAs FET arrays, without examination of the processes involved for their sensitivity features, were obtained earlier [9]. To the moment FET detectors also have rather appropriate characteristics (NEP_{opt} ~$10^{-10}\ldots10^{-11}$ W/Hz$^{1/2}$ in dependence of channel dimensions, radiation frequency regions, antenna-detector matching, *etc.*).

Physics of Si-FET and HFET detectors is a little bit different (*e.g.*, Si FETs operate in the inversion region but HFETs operate in the accumulation region). For HFETs, the model parameters are not so properly developed as for Si MOSFETs. Because of it, below it is accepted that some parameters of HFETs can be taken similar to those of Si MOSFETs devices.

The detectors under consideration have strong dependence NEP$_{opt}(\nu)$ (NEP$_{opt} \sim \nu^m$) and responsivity $\Re \sim \nu^{-m}$, where m = 2…4 [7, 10-12]). Majority of them can be produced at foundry level as their technology readiness level is high. At low radiation powers they are square-law detectors in which the DC voltage response is proportional to the incoming signal power. As compared to the thermal THz uncooled detectors, the rectifying ones have a wider dynamic range. Relatively low noise (when being zero biased [13]), small dimensions, and availability of technologies make these detectors favorable for sub-THz/THz wave detection. All these rectifying detectors are rather fast (the response time $\tau \le 10^{-9}$ s in Si MOSFET detectors [14], $\tau \le 10^{-11}$ s in GaAs uncooled FETs [15], $\tau \le 10^{-11}$ s in SBDs [16]). As direct detection detectors, they can operate in wide spectral ranges (for Si MOSFET detectors $\nu \le 9$ THz [14], for GaAs FETs $\nu \le 22$ THz [12] and for SBDs $\nu \le 10$ THz [17]).

The important task for application of these detectors, *e.g.*, in direct detection vision systems, is estimation of their upper limit performance parameters ($\Re_{opt}$ and NEP$_{opt}$).

Rectifying THz FET (HFET) or SBD detectors consist of the sensitive non-linear element (gate-source contact at FET (HFET) channel or metal-semiconductor junction, respectively), parasitic elements and antenna. FET and HFET detectors considered are direct detection rectifying detectors with broadband (non-resonant) detection [18] when their channel length L is larger than the short channel distance near the source L_{eff}. Within the $L_{eff} = \sqrt{\frac{\sigma_{CH}\cdot L^2}{\omega\cdot C_{CH}}}$, rectification occurs, and it is of the order of few tens nanometers [19]. Here, $\sigma_{CH} = \left.\frac{\partial I_{DS}}{\partial V_{DS}}\right|_{V_{DS}=0V}$ is the channel conductivity, I_{DS} is the drain-source current and C_{CH} is the channel capacity, $\omega = 2\pi\nu$.

These detectors will be considered here at zero bias, since the nonzero bias will lead to additional noise in FET detectors almost not improving their NEP [13]. Conventional SBD detectors (*e.g.*, GaAs SBDs) for effective power matching, because of high junction resistance, are forward biased though such biasing leads to an additional $1/f$ noise. For SBDs based on ternary III-V semiconductor alloys (*e.g.*, InGaAs/InP SBDs [20, 21]), when Schottky potential barrier is lowered, the impedance at zero bias is much lower, as compared to that in GaAs or Si SBDs.

2. Currents and voltages

Density plasma perturbations lead to rectification of high frequency radiation at G-S (gate-source) contacts that gives the feasibility to consider FET as an electronic circuit using its current-voltage non-linear characteristics.

The usage of current-voltage characteristics allows to include into consideration also diffusion current, which is important because, as a rule, the maximum output signal of FET THz detectors is observed at G-S biases where both drift and diffusion currents should be taken into account [7].

For rectifying detectors, an important issue to get optical noise equivalent power NEP$_{opt}$ values is the necessity of accounting the antenna Z_A impedance and that of the detector Z_{det} with its extrinsic parasitics X_P, R_S and the load impedance Z_L (see Fig. 1)

$$Z_{det}(x,\omega) = R_S + \frac{X_P(\omega)\cdot Z_{INT}(x,\omega)}{X_P(\omega)+Z_{INT}(x,\omega)}, \qquad (1)$$

where R_S and $X_P = -\frac{j}{\omega\cdot C_P}$ are the parasitic series resistance and parasitic shunt capacitance, respectively, C_P is the shunt capacity, $j = (-1)^{1/2}$, the parameter $x = \frac{V_{GS}-V_{TH}}{n\cdot\varphi_t}$ or $x = \frac{V_D}{n\cdot\varphi_t}$ for FET (HFET) and SBD detectors, respectively, $\varphi_t = \frac{k_B \cdot T}{q}$ is the thermal potential, V_{TH} is the threshold voltage, V_{GS} is the gate-source voltage and the slope of current-voltage characteristics in FETs or ideality factor in SBDs $n \approx 1\ldots10$ (at room temperature $n \sim 1.3\ldots1.5$ for Si MOSFETs [7], $n \sim 1.1\ldots1.3$ for SBDs [16], $n \sim 2$ and $n \sim 10$ for GaAs and GaAlN HFETs [18], respectively), $Z_{INT} = Z_{GS,int}$, where $Z_{GS,int}$ is the internal source-gate impedance. In the case of SBDs $Z_{INT} = R_D$, where R_D is the SBD differential active resistance. In Fig. 1, the ΔV_0 value indicates the signal amplitude. The parameters X_P, Z_A and Z_{INT} are dependent on the radiation frequency ν.

In the pioneering paper [8] and some publications (see, e.g. [18, 22, 23]), attention primarily was concentrated on the electrical $\Re_{el}$ responsivity or electrical NEP$_{el}$ rather than on the optical NEP$_{opt}$. The latter one takes into account the antenna properties, its matching efficiency with detector, the extrinsic parasitics, and matching with the measuring facility. For FETs and SBDs, the values of NEP$_{opt}$ > NEP$_{el}$ (NEP$_{opt}$ is worse as compared to NEP$_{el}$) [7, 22-24].

In SBDs, the diode current $I = I_D$ is dependent on the forward bias $V = V_D$ as [25]

$$I_D(x) = I_0 \cdot f_D(x)\,, \tag{2}$$

$$I_0 = I_{0,SBD} = \frac{4 \cdot \pi \cdot S_D \cdot q^3 \cdot m^* \cdot e^{-\frac{\varphi_B(0)}{n \cdot \varphi_t}}}{h^3} \cdot \varphi_t^2\,, \tag{3a}$$

$$f_D(x) = e^x - 1. \tag{3b}$$

Here, S_D is the diode area, q – electron charge, $\varphi_B(0)$ – Schottky barrier height, m^* – electron effective mass, and h – Plank constant.

In FETs, the channel current I_{DS} can be presented as [7, 26]

$$I_{DS}(x, y) = I_0 \cdot f_{DS}(x, y)\,, \tag{4}$$

$$I_0 = I_{0,\,FET} = \frac{W}{L} \cdot \mu_n \cdot C'_{ox} \cdot n \cdot \varphi_t^2\,, \tag{5}$$

$$f_{DS}(x, y) = 2 \cdot \left[\left(\ln\left(1 + e^{\frac{x}{2}}\right)\right)^2 - \left(\ln\left(1 + e^{\frac{x-y}{2}}\right)\right)^2\right], \tag{6}$$

where x and $y = \frac{V_{DS}}{\varphi_t}$ are dimensionless parameters, V_{DS} is the drain-source voltage, W and L are the channel width and length, respectively, μ_n (cm^2/(V·s)) is the electron mobility in the channel, C'_{ox} (F/cm^2) is the specific surface capacity of the metal-dielectric-semiconductor structure.

Under the THz radiation with the frequency ω and arising high frequency voltage signal $\Delta V_0 \cdot \sin(\omega \cdot t)$ between the detector terminals (Fig. 1), the device rectified current δI_{SBD} can be found using the Taylor series at low level signals ($\Delta V_0 <\sim n\phi_t$) and the time averaging. In the case of SBDs [27],

$$\delta I_{SBD} = \frac{\Delta V_0^2}{4} \cdot \left.\frac{d^2 I_D}{dV_D^2}\right|_{V_D=0}. \tag{7}$$

For the channel rectified current δI_{FET} in FETs (see, *e.g.*, [7, 28])

$$\delta I_{\text{det\_}FET} = \frac{\Delta V_0^2}{4} \cdot \left[\left.\frac{\partial^2 I_{DS}}{\partial V_{GS}^2}\right|_{\substack{V_{GS}=V_{GS}\\ V_{DS}=0}} + \delta_{GD}^2 \cdot \left.\frac{\partial^2 I_{DS}}{\partial V_{DS}^2}\right|_{\substack{V_{GS}=V_{GS}\\ V_{DS}=0}} + 2 \cdot \left.\frac{\partial^2 I_{DS}}{\partial V_{GS} \partial V_{DS}}\right|_{\substack{V_{GS}=V_{GS}\\ V_{DS}=0}} \cdot \delta_{GD} \cdot \cos(\Delta\phi)\right] \tag{8}$$

The term $\frac{1}{2}\left.\frac{\partial^2 I_{DS}}{\partial V_{GS}^2}\right|_{\substack{V_{GS}=V_{GS}\\ V_{DS}=0}} = 0$ is zero, when $V_{DS} = 0$ V, $\Delta\phi$ is the phase of the drain-source perturbation $\Delta V_{DS} \cdot \sin(\omega \cdot t + \Delta\phi)$ from the signal $\Delta V_0 \cdot \sin(\omega \cdot t)$, the parameter $\delta_{GD} = \Delta V_{DS}/\Delta V_0$. In the simplified one-dimensional model of the FET equivalent circuit, the values $\Delta\phi = 0$ and $\delta_{GD} = 1$ [7, 28].

In general case for FETs and SBDs from Exps. (2)-(8), the device rectified current δI_{det} can be found as

$$\delta I_{det} = \frac{\Delta V_0^2}{4} \cdot \frac{1}{n \cdot \varphi_t} \cdot \sigma_0 \cdot \frac{\partial f_\sigma(x)}{\partial x}(2 - n). \tag{9}$$

For SBDs with zero bias ($V_D = 0$), the parameter $\sigma_0 = \sigma_{0,SBD} = \frac{I_0}{n \cdot \varphi_t}$ is the differential conductivity of the metal-semiconductor contact and the dimensionless expression

$$\frac{\partial f_\sigma(x)}{\partial x}(2 - n) = 1\,. \tag{10}$$

For FETs (HFETs) $\sigma_0 = \sigma_{0,\,FET} = I_0/\varphi_t$ is the coefficient that characterizes the channel conductivity and $f_\sigma(x)$ is the dimensionless parameter that takes into account the conductivity changes in the gate-source voltage V_{GS}

$$f_\sigma(x) = \frac{\partial f_{DS}(x, 0)}{\partial y} = \frac{2 \cdot \ln\left(1 + e^{\frac{x}{2}}\right) \cdot e^{\frac{x}{2}}}{\left(1 + e^{\frac{x}{2}}\right)}. \tag{11}$$

The term $(2–n)$ in Exp. (9) is zero, when coefficient $n = 2$. It means that FET devices (for example GaAs FETs at room temperature [18]) with $n \sim 2$ could have low responsivity. Relatively low sensitivity of this kind devices was observed in [12], where ultrafast THz radiation detection of large area GaAs FETs was investigated. Also, it should be taken into account that, at first, the equations (4)–(6) were taken really for MOSFET (where $n \sim 1.3\ldots1.5$) and did not include all types of FETs. Therefore, the coefficient n could have different contribution to the final signal. Second, the conditions $\Delta\phi = 0$ and $\delta_{GD} = 1$ in Eq. (8) are true in the simplified equivalent circuit transistor model only, *e.g.*, inductances can contribute, too, but were not taken into account. Finally, it is difficult to set the experiments with different type of transistors but with the same antennas and matching impedance conditions. Frequently, the authors (see, *e.g.*, [23, 28]) to avoid the uncertainties assume the expression $(2–n) = 1$.

For estimations of the upper limit performance of the detectors in the course of calculations, in this paper it was used $n = 1.3$ (Si MOSFET, that was obtained in our examination of Si MOSFET C-V characteristics), $n = 5$ (AlGaN HFET, from our analysis of C-V characteristics of the investigated transistors), and $n = 1$ for SBDs.

The detector voltage δV_{det} conditioned by current δI_{det} is

$$\delta V_{det} = \frac{\delta I_{det}}{\sigma_0 \cdot f_\sigma(x)} \cdot \eta_L(x, \nu_m), \tag{12}$$

where $f_\sigma(x) = 1$ for SBDs at zero bias.

The coefficient η_L (Fig. 1a) takes into account the voltage divider between the detector resistance and the load impedance Z_L of the registration system

$$\eta_L(x, \nu_m) = \left| 1 + \frac{1}{\sigma_0 \cdot f_\sigma(x) \cdot Z_L(\nu_m)} \right|^{-1}, \tag{13a}$$

$$Z_L(\nu_m) = \frac{R_L \cdot X_L(\nu_m)}{R_L + X_L(\nu_m)}, \tag{13b}$$

$$X_L(\nu_m) = -\frac{j}{2\pi \cdot \nu_m \cdot C_L}. \tag{13c}$$

Here R_L, X_L, and C_L are the load resistance, capacitance, and capacity, respectively.

The interconnection between the detector signal voltage amplitude ΔV_0 and the radiation power falling down onto detectors, can be determined from the electrical circuit shown in Fig. 1. THz radiation that is received by the antenna with the impedance Z_A generates the high frequency voltage with the amplitude V_A in the antenna-detector circuit.

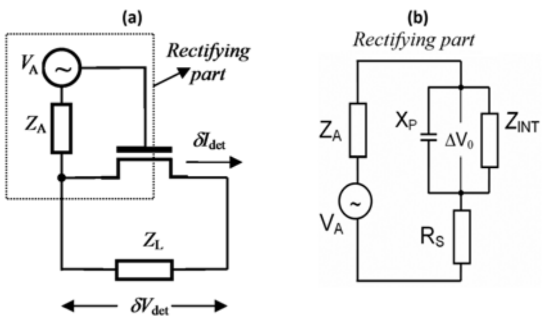

Fig. 1. Schematic view of the FET THz detector with external load impedance Z_L (*a*), and simplified schematic representation of rectifying THz detector taking into account the basic extrinsic parasitic components (*b*).

In SBDs, the internal impedance is the differential resistance of the metal-semiconductor contact [27] $Z_{int} = 1/\sigma_0$. In FETs, the internal impedance can be calculated in approximation of double-pass line with distributed parameters [7, 28]

$$Z_{int}(x, \omega) = Z_{GS,int}(x, \omega) = \sqrt{\frac{1}{2 \cdot \sigma_{CH}(x) \cdot \omega \cdot C_{CH}}} \cdot (1 - j) \tag{14}$$

where $\sigma_{CH} = \sigma_0 \cdot f_\sigma(x)$, $C_{CH} \approx W \cdot L \cdot C'_{ox}$ (in strong inversion regime) are the channel conductivity and capacity of FET channel, respectively.

Taking into account the circuit in Fig. 1b, it can be found the detector rectified voltage

$$\Delta V_0^2(x) = \xi_Z(x) \cdot V_A^2 = \left| \frac{X_P \parallel Z_{\text{int}}(x)}{Z_A + R_S + X_P \parallel Z_{\text{int}}(x)} \right|^2 \cdot V_A^2, \tag{15}$$

where ξ_Z is the transfer coefficient of the square voltage from the antenna to transistor, V_A is the antenna voltage.

3. Responsivity and NEP

The antenna impedance can be written as [29]

$$Z_A = R_A + j \cdot X_A = R_{A,R} + R_{A,L} + j \cdot X_A, \tag{16}$$

where R_A and X_A are the real and imaginary parts, respectively, $R_{A,R}$ is the radiation antenna resistance, and $R_{A,L}$ is the resistance of losses. The antenna voltage V_A is

$$V_A = E_{THz} \cdot l_A = E_{THz} \cdot \lambda \cdot \sqrt{\frac{R_{A,R} \cdot D_0}{\pi \cdot Z_0}}, \tag{17}$$

where E_{THz} is the field and

$$l_A = \lambda \cdot \sqrt{\frac{R_{A,R} \cdot D_0}{\pi \cdot Z_0}} \tag{18}$$

is the dipole antenna effective length [30], $Z_0 \approx 377\ \Omega$ is the free-space impedance, λ is the radiation free-space wavelength, and D_0 is the antenna directivity coefficient.

According to the equations (15), (17), and (18)

$$\frac{E_{THz}^2}{Z_0} = \frac{V_A^2}{R_{A,R}} \cdot \frac{\pi}{\lambda^2 \cdot D_0} = \frac{\Delta V_0^2}{R_{A,R}} \cdot \frac{\pi}{\lambda^2 \cdot D_0} \cdot \frac{1}{\xi_Z} \tag{19}$$

The radiation power P_{opt} falling down onto detector area A_{opt} is as follows

$$P_{opt} = W_{THz} \cdot A_{opt} = \frac{E_{THz}^2}{2 \cdot Z_0} \cdot A_{opt} = \frac{V_A^2}{8 \cdot R_{A,R}} \cdot \frac{4\pi \cdot A_{opt}}{\lambda^2 \cdot D_0}, \tag{20}$$

where W_{THz} is the power density of the electromagnetic wave. Then, for the current optical responsivity $\Re_{I,opt} = \delta I_{det} / P_{opt}$ from Exps. (9) and (20) it follows in the form of similar Exps. for SBD and FET detectors

Semiconductor Physics, Quantum Electronics & Optoelectronics, 2016. V. 19, N 2. P. 129-138.
doi: 10.15407/spqeo19.02.129

$$\Re_{I,opt} = \frac{2 \cdot R_{A,R} \cdot \sigma_0}{\varphi_t} \cdot \left| \frac{2-n}{n} \right| \cdot f_\sigma' \cdot \xi_Z \cdot \xi_{opt} \cdot D_0 , \qquad (21)$$

and for the voltage optical responsivity $\Re_{V,opt} = \delta V_{det}/P_{opt}$

$$\Re_{V,opt} = \frac{2 \cdot R_{A,R}}{\varphi_t} \cdot \left| \frac{2-n}{n} \right| \cdot \frac{f_\sigma'}{f_\sigma} \cdot \eta_L \cdot \xi_Z \cdot \xi_{opt} \cdot D_0 , \qquad (22)$$

where the coefficient $\xi_{opt} = \dfrac{\lambda^2}{4\pi \cdot A_{opt}}$ characterizes the efficiency of antenna (like an aperture efficiency in [29]), and $f_\sigma' = d\, f_\sigma / dx$.

The optical $\mathrm{NEP}_{opt} = V_{noise}/\Re_{V,opt}$ expression for a minimal noise that is the Johnson–Nyiquist noise [13, 31] in FETs at zero bias $V_{DS} = 0$ and SBDs at $V_D = 0$

$$V_{noise} = \sqrt{4 \cdot k_B \cdot T \cdot \left(r_{dsw} \cdot W^{-1} + R_0 \cdot f_\sigma^{-1} \right)} = \\ = 2 \cdot q^{1/2} \cdot \varphi_t^{1/2} \cdot \left(r_{dsw} \cdot W^{-1} + R_0 \cdot f_\sigma^{-1} \right)^{1/2} \qquad (23)$$

is

$$\mathrm{NEP}_{opt} = \frac{q^{1/2} \cdot \varphi_t^{3/2} \cdot R_0^{1/2}}{R_{A,R}} \cdot \left| \frac{n}{2-n} \right| \times \\ \times \left(\frac{r_{dsw}}{R_0 \cdot W} + \frac{1}{f_\sigma} \right)^{1/2} \cdot \frac{f_\sigma}{f_\sigma'} \cdot \frac{1}{\xi_Z \cdot \xi_{opt} \cdot D_0} . \qquad (24)$$

Here, the resistance $R_0 = 1/\sigma_0$. The parameter η_L in Exp. (13a) depends on the registration setup, and for upper limit performance estimations it was taken $\eta_L = 1$.

For FETs, r_{dsw} is the resistance per unit transistor width between the source and drain areas (except channel resistance), Ω·µm. The parameter r_{dsw} was taken from BSIM3.3, BSIM4 models for MOSFETs or from I-V FET characteristics.

This coefficient can play a substantial role in devices with high electron mobility. In Si MOSFETs its influence is less noticeable, as the channel resistance influence is much more important. The minimum value of the function $f_\sigma^{1/2}/f_\sigma' \approx 1.75$ and the maximum value of the function $f_\sigma'/f_\sigma = 1$ defines the optimum NEP_{opt} and sensitivity $\Re_{V,opt}$ values, respectively.

For zero biased SBDs, the ratio $\dfrac{r_{dsw}}{W}$ is $\dfrac{r_{dsw}}{W} = R_s$, the parameter $\left| \dfrac{n}{2-n} \right|$ should be changed to n, and the functions values $f_\sigma = f_\sigma^{1/2} = f_\sigma' = 1$.

It follows that the ultimate value of NEP_{opt} for MOSFET THz detectors in low radiation frequency limit (ν ~<300 GHz) should be worse by a factor of ~1.75 as compared to SBD ones (not taking into account their radiation frequency dependences), when their impedances are comparable in value, and comparable are the antenna impedances.

The ultimate $\Re_{V,opt}$ and NEP_{opt} values follows from (22) and (24), respectively,

$$\Re_{V,opt} \approx 23\ \text{kV/W},\ \mathrm{NEP}_{opt} \approx \frac{f_\sigma^{1/2}}{f_\sigma'} \cdot 10^{-12}\ \text{W/Hz}^{1/2} \qquad (25)$$

under the assumptions that $n = 1$, $R_{A,R} = 300\ \Omega$, $T = 300$ K, $R_0 = 10^4\ \Omega$, $\xi_Z = \xi_{opt} = D_0 = 1$, $r_{dsw} = 0\ \Omega\cdot\mu$m. The coefficient ξ_Z is dependent on the mismatch of the antenna-detector impedance and can be improved by introducing some compensating elements (*e.g.*, inductances). The coefficient ξ_{opt} can be higher or lower as compared to unity and is dependent on detector and antenna design. The directivity D_0 can be >> 1, but for vision systems with relatively large arrays it should not be high. The values $\Re_{V,opt} \approx 5$ kV/W were earlier observed [19].

4. THz rectifying detector parameters

One of the important FET (HFET) THz detector parameters is the channel resistance $R_0 = L/\left(W \cdot \mu_n \cdot C_{ox}' \cdot n \cdot \varphi_t\right)$ [26] which is in direct proportion to the channel length L, and inversely proportional to the channel width W and mobility μ_n. To reduce R_0 (*e.g.*, reducing the Johnson–Nyiquist noise) the length L is designed as small as it is allowed by manufacturing design rules (but $L > L_{eff}$). The width W can be optimized to get better NEP_{opt} performance. To decrease the resistance R_0, the width W should be increased. At the same time, the width W cannot be very wide, as the gate parasitic serial resistance R_S becomes large [32]

$$R_S = r_0 + r_1/W + r_2 \cdot W/(3 \cdot L), \qquad (26)$$

where r_0 is the resistance of the contacts between the metal and gate layers (~5 Ω), r_1 – transistor source resistance ($r_1 = r_{dsw}/2$, typically $r_1 \sim 400\ \Omega\cdot\mu$m for Si MOSFETs) and r_2 is the gate material resistance. For example, for III-V HFETs (*e.g.*, AlGaN/GaN HFET) in which the gate is due to a Schottky barrier, its metallic gate resistance r_2 is considerably smaller than the polysilicon gate resistance in Si MOSFETs.

Typically, in Si MOSFETs r_1 and r_2 values are as follows: $r_1 \sim 400\ \Omega\cdot\mu$m, $r_2 \sim 40\ \Omega$ (*e.g.*, in the 0.35 µm technology design rules), and in AlGaN/GaN HFETs the value $r_2 < 0.5\ \Omega$. To avoid power losses, the value of R_S has to be smaller than the antenna radiation resistance $R_{A,R}$ ($R_{A,R} \sim 100…300\ \Omega$ (in dependence on the antenna type [14, 23]).

The channel width W is also limited by parasitic shunt capacitance X_P between the transistor gate and source. It is dependent on radiation frequency ν, the shunting capacity C'_P per unit width (it is equal to *cgdo* or *cgso* parameters in BSIM3.3, BSIM4 models), and the width W [7]

$$X_P = -j/(2 \cdot \pi \cdot \nu \cdot W \cdot C_P') . \qquad (27)$$

The C_P' values depend on design rules production technology (*e.g.*, $C_P' \approx 2\cdot 10^{-10}$ F/m for 0.35 µm Si MOSFET design rules). In estimations it is assumed that the influence of the channel width W on capacitance X_P for AlGaN/GaN HFETs and Si MOSFETs is similar.

Calculated NEP$_{opt}$ dependences for Si MOSFET direct detection detectors on channel width W for different radiation frequencies ν and parameters used from BSIM3.3, BSIM4 models are presented in Fig. 2.

From Fig. 2, one can note the strong dependences of the optimal NEP$_{opt}$ on the channel width at different radiation frequencies. The minimum NEP$_{opt}$ is shifted with ν growth to shorter W. For the radiation frequency range of ~0.5 THz for Si MOSFETs the optimum channel width W_{opt} in the long channel approximation should be about 700 nm. For the 4 THz radiation frequency range, it should be W ~300 nm.

The optimum NEP$_{opt}$ is also shifted to better (lower) values with the antenna resistance $R_{A,R}$ shift from $R_{A,R} = 100\ \Omega$ for dipole antenna up to $R_{A,R} = 300\ \Omega$ [14, 23] for patch antenna.

NEP$_{opt}(W)$ dependences at T = 300 K for AlGaN/GaN HFETs with the channel length L = 0.25 μm (0.25 μm technology) are shown in Fig. 3. One can see the strong dependences on W and ν. AlGaN/GaN HFETs seem to be better compared to Si MOSFETs for low radiation frequency regions (ν < 300 GHz) and comparable devices noise, and Si MOSFETs can be better for higher radiation frequency range because of larger series resistance in AlGaN/GaN HFETs between the source and drain. It seems that the requirements to the channel length for AlGaN/GaN HFETs as THz detectors are less rigorous as compared to Si MOSFET detectors.

From comparison of Figs 2 and 3, one can see that because of different parameters for Si FETs and AlGaN/GaN HFETs optimal W for their NEP$_{opt}$ is different: for optimal NEP$_{opt}$ of AlGaN/GaN HFETs the channel width should be several times wider as compared to Si FETs channel width, which is mainly related with larger source-gate resistance in AlGaN/GaN HFETs (due to larger distances between the source and gate in AlGaN/GaN HFETs). It is also seen that the optimal gate voltages V_{GS}, to get better NEP$_{opt}$ for these two types of rectifying detectors, are different. For Si FETs, at which the detector operation is optimal, the V_{GS} ranges are wider.

In III-V HFET THz detectors, it seems that NEP$_{opt}$ can be worse as compared to that one in Si MOSFETs, since III-V HFETs tend to have larger 1/f noise, and, thus, it is more difficult to reach the detectors fundamental thermal noise (Johnson–Nyiquist noise) limit that insures the lowest possible NEP$_{opt}$. But HFET models are not well developed as compared to Si MOSFET models with parameters proven in them.

The calculated and known experimental NEP$_{opt}$ data for Si MOSFET THz detectors are presented in Fig. 4. Numbers at the experimental points mean the Ref. numbers in the list of Refs. The curves for different radiation frequencies were recalculated for the detector

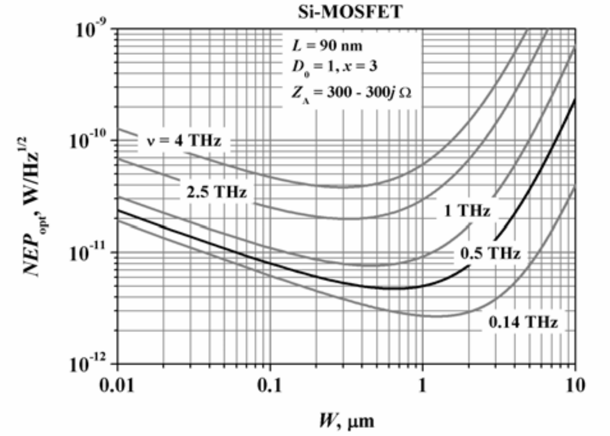

Fig. 2. Optimization of Si MOSFET width W at different radiation frequency ν by minimum NEP$_{opt}$ values. Si MOSFET: T = 300 K, L = 90 nm, C'_{ox} = $4.5\cdot10^{-3}$ F/m^2, C'_P = $2\cdot10^{-10}$ F/m, n = 1.3, x = 3, μ_n = 400 cm^2/V·s, Z_A = 300 – 300·j Ω, r_{dsw} = 800 Ω·μm, r_0 = 5 Ω, r_1 = 400 Ω·μm, r_2 = 45 Ω, $\xi_{opt} = D_0 = 1$.

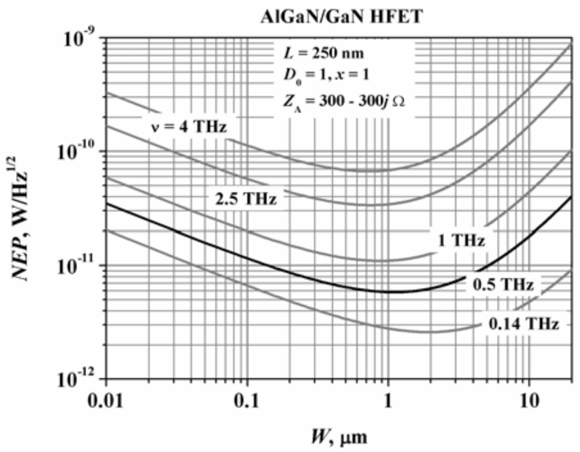

Fig. 3. NEP$_{opt}$ of GaAlN/GaN HFETs as a function of the channel width W with the channel length L = 0.25 μm (0.25-μm technology). T = 300 K, n = 1.3, Z_A = 100 – 100·j. For optimal NEP$_{opt}$, it is taken that x = 1.

antenna area $\lambda^2/4\pi$ instead of smaller physical area of the patch antennas used for obtaining NEP$_{opt}$ in [14].

Antenna impedance Z_A = 300...300·j Ω [14] was taken for patch antenna. Calculations were fulfilled for the optimal NEP$_{opt}$ channel width, which is dependent on the radiation frequency, as it is shown in Fig. 2. For comparison, in Fig. 4 it is also presented the calculated NEP$_{opt}$ radiation frequency dependence for the constant value W = 120 nm.

NEP$_{opt}$ ≈ $2\cdot10^{-10}$ W/Hz$^{1/2}$ values at ν ≈ 150 GHz obtained here for Si-MOSFETs at T = 300 K with non-optimized antennas are away of performance limits shown in Fig. 4. These data are not shown in Fig. 4, though they are within a lot of data known for this kind of THz detectors.

Semiconductor Physics, Quantum Electronics & Optoelectronics, 2016. V. 19, N 2. P. 129-138.
doi: 10.15407/spqeo19.02.129

The NEP$_{opt}$ dependences that are presented for a simplified circuit with the extrinsic parasitics shown in Fig. 1 don't take into account a number of parasitics inherent to these devices [26], which will worsen (increase) NEP$_{opt}$. Their inclusion requires more complicated modeling. The dependences presented indicate the upper limit performance for such kind of devices as THz detectors.

In Fig. 5, the calculated NEP$_{opt}$(ν) dependences for SBD THz detectors and the best known experimental data are presented. Numbers at experimental points mean the Ref. numbers in the list of Refs. One can see rather reasonable matching of calculated curves with the known experimental data for the models that takes into account only extrinsic parasitic components. The curves I and III were calculated not taking into account the compensating influence of the antenna impedance $Z_A = 26 + 175j\ \Omega$ at radiation "resonance" frequency $\nu \approx 90$ GHz, which compensates the detector impedance $Z_{SBD} = 26 - 175j\ \Omega$ at this frequency (when only active and capacity components are included) explaining the low NEP$_{opt}$ in this frequency range (curve IV). But for other radiation frequencies, the values of NEP$_{opt}$ for these "resonant" detectors will be much worse, as compared to those where the compensating inductance is not included, because of the antenna radiation frequency impedance mismatch with the detector impedance.

Comparing the *NEP$_{opt}$* radiation spectral dependences for FET and SBD detectors shown in Figs 4 and 5, one can note the stronger dependence of NEP$_{opt}$ on ν in SBD THz detectors (it was noted $\Re_{opt} \sim \nu^{-4}$ [17]), which is related with that in Z_{INT}, as the capacity is absent in SBDs (only an active resistance is present). Because of it, within the considered models, FET detectors can be preferable over SBD ones in the radiation frequency range $\nu > 500$ GHz. At lower radiation frequencies, SBD direct detection detectors can get better parameters.

In FET (HFET) detectors, to our knowledge, there were not considered the circuits with compensating inductive elements for antenna impedance, which improves the antenna-detector matching at a certain resonance radiation frequency.

The dependences of NEP$_{opt}$(ν) for AlGaN/GaN HFETs are not presented here because of the lack of enough number of experimental data, except the known data [47-51], but these data are away from the calculated ones, and they were obtained not for optimal *W* values and, as a rule, they were obtained for unknown antenna parameters. Some parameters used for NEP$_{opt}$ estimations were taken the same as for Si MOSFET and thus are not fully appropriate. The obtained here at $\nu \approx 150$ GHz NEP$_{opt}$ $\approx 10^{-10}$ W/Hz$^{1/2}$ values without antennas are away of ultimate performance data estimated in Fig. 3.

To the moment, from the above analysis it is seen that these uncooled direct detection rectifying detectors can be only used in active imaging systems, as their NEP$_{opt}$ are away, at least, of NEP$_{opt}$ < (10^{-13}…10^{-14}) W/Hz$^{1/2}$ value needed [52] for direct detection passive imaging systems.

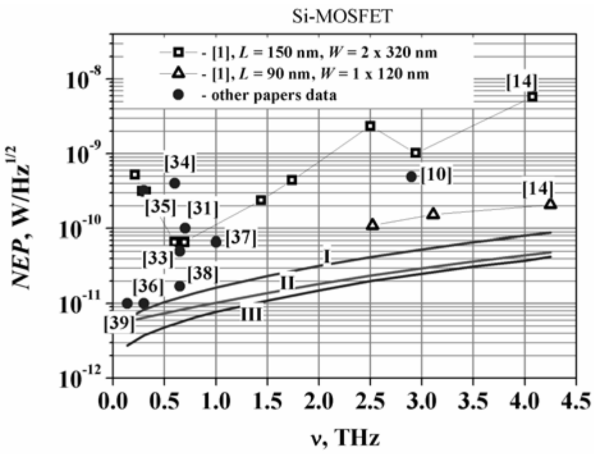

Fig. 4. Experimental values of NEP$_{opt}$ from [14] for Si FETs were recalculated for antenna area $\lambda^2/4\pi$ instead of physical area of the patch antennas used in [14] (antenna impedance $Z_A = 300...300{\cdot}j\ \Omega$). The calculated curves (L = 90 nm, D_0 = 1): I – for the optimal width W, $Z_A = 100 - 100{\cdot}j\ \Omega$; II – for W = 1×120 nm, $Z_A = 300 - 300{\cdot}j\ \Omega$; III – W is the optimal width, $Z_A = 300 - 300{\cdot}j\ \Omega$. Data from other papers were represented as they are. The calculations were fulfilled for optimal for *NEP$_{opt}$* channel width that is dependent on the radiation frequency (see Fig. 2).

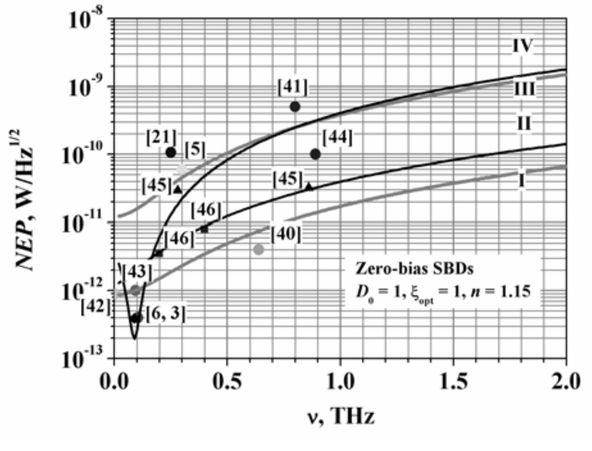

Fig. 5. Experimental values NEP$_{opt}$ of the SBD and results of the calculation (curves I–IV) according to Eq. (24) under the assumptions $D_0 = 1$, $\xi_{opt} = 1$, $n = 1.15$. I – $R_j = 2.9$ kΩ, $C_j = 5$ fF, $R_s = 45\ \Omega$, $Z_A = 100\ \Omega$ (InGaAs SBD, parameters from [46]); II – $R_j = 2.9$ kΩ, $C_j = 5$ fF, $R_s = 45\ \Omega$, $Z_A = 100 - 100{\cdot}j\ \Omega$ (InGaAs SBD, parameters from [46]); III – $R_j = 700$ kΩ, $C_j = 8$ fF, $R_s = 10\ \Omega$, $Z_A = 100\ \Omega$ (Si SBD, parameters from [45]), IV – $R_j = 2.4$ kΩ, $C_j + C_P = 7.1$ fF, $R_s = 5.5\ \Omega$, $Z_A = 24 + 231{\cdot}j\ \Omega$ (InGaAs SBD, parameters from [6], resonant impedance matching at 89 GHz). The values NEP$_{opt}$ for Si SBD from [45] were shown, as it is in the bias regime when $R_j = 600\ \Omega$ (instead of 700 kΩ in the zero-bias regime that was taken to calculate the curve III).

5. Conclusions

The responsivity $\Re_{opt}$ and the noise equivalent power NEP$_{opt}$ of a long channel ($L > L_{eff}$) for unbiased (zero drain-source bias $V_{DS} = 0$) uncooled FETs, HFETs and SBDs ($V_D = 0$) as THz detectors were considered within the similar models in the frame of current-voltage characteristics taking into account the basic parasitic components (active resistance and capacities). It was concluded that, with account of the antenna-detector impedance matching, it is possible to estimate FET, HFET and SBD THz detectors ultimate performance limits choosing the optimal channel width W at different radiation frequencies ν and antenna coupling with the detector. NEP$_{opt}$ strong dependences on channel width in Si MOSFET and HFET THz detectors are predicted.

At the low radiation frequency limit, the estimated NEP$_{opt}$ and responsivity $\Re_{opt}$ for FET detectors can achieve values NEP$_{opt}$ ~ 10^{-12} W/Hz$^{1/2}$ and $\Re_{opt}$ ~ 23 kV/W. The ultimate NEP$_{opt}$ values of FET detectors are worse by a factor of ~1.75, as compared to the SBD ones (in the low radiation frequency range ν < 300 GHz), when these devices and antenna impedances are comparable in values. With the parameters pointed out, the uncooled direct detection detectors can be only used in active imaging systems.

Some part of the paper content concerning Si MOSFET THz detectors was presented in [53].

References

1. D. Saeedkia (ed.), *Handbook of Terahertz Technology for Imaging, Sensing and Communications*. Woodhead Publishing, Oxford, Cambridge, Philadelphia, New Delhi, 2013.
2. C.M. Armstrong, The truth about terahertz // *IEEE Spectrum*, September, p. 36-41 (2012).
3. H. Kazemi, G. Nagy, L Tran et al., Ultra sensing ErAs/InAlGaAs direct detectors for millimeter wave and THz imaging applications // *IEEE/MTT-S International Microwave Symposium*, Honolulu, HI, June 3–8, 2007, p. 1367-1370.
4. J.L. Hesler and T.W. Crow, Responsivity and noise measurements of zero-bias Schottky diode detectors // *Proc. IRMMW-THzTech*, Cardiff, UK, Sept. 3-7, 2007, pp. 844-845.
5. H. Liu, J. Yu, P. Huggard, and B. Alderman, A multichannel THz detector using integrated bow-tie antennas // *Int. J. Antennas Propag*. 417108 (2013).
6. M. Hoefle, K. Haehnsen, I. Oprea et al., Compact and sensitive millimetre wave detectors based on low barrier Schottky diodes on impedance matched planar antennas // *J. Infrared Milli Terahz Waves*, **35**, p. 891-908 (2014).
7. M. Sakhno, A. Golenkov and F. Sizov, Uncooled detector challenges: Millimeter-wave and terahertz long channel field effect transistor and Schottky barrier diode detectors // *J Appl. Phys*. **114**, 164503 (2013).
8. M. Dyakonov and M. Shur, Plasma wave electronics: Novel terahertz devices using two dimensional electron fluid // *IEEE Trans. Electron Devices*, **43**, p. 1640-1645 (1996).
9. W. Chew and H. R. Fetterman, Millimeter wave imaging using FET detectors integrated with printed circuit antennas // *Int. J. Infr. Milli. Waves*, **10**, p. 565-578 (1989).
10. S. Boppel, A. Lisauskas, M. Mundt et al., CMOS Integrated antenna-coupled field-effect transistors for the detection of radiation from 0.2 to 4.3 THz // *IEEE Trans. Microw. Theory Techn*. **60**, p. 3834-3843 (2012).
11. D.B. But, C. Drexler, M.V. Sakhno et al., Nonlinear photoresponse of field effect transistors terahertz detectors at high irradiation intensities // *J. Appl. Phys*. **115**, 164514 (2014).
12. S. Regensburger, M. Mittendorff, S. Winnerl et al., Broadband THz detection from 0.1 to 22 THz with large area field-effect transistors // *Opt. Express*, **23**, No.16, p. 20732-20742 (2014).
13. A. Lisauskas, S. Boppel, J. Matukas, V. Palenskis, L. Minkevicius, G. Valusis, P. Haring-Bolıvar, and H. G. Roskos, Terahertz responsivity and low-frequency noise in biased silicon field-effect transistors // *Appl. Phys. Lett*. **102**, 153505 (2013).
14. A. Lisauskas,·M. Bauer,·S. Boppel et al., Exploration of terahertz imaging with silicon MOSFETs // *J Infrared Milli Terahz Waves*, **35**, p. 63-80 (2014).
15. S. Preu, M. Mittendorf, S. Winnerl, H. Lu, A.C. Gossard, and H. B. Weber, Ultra-fast transistor-based detectors for precise timing of near infrared and THz signals // *Opt. Express*, **21** (15), p. 17941-17950 (2013).
16. L. Liu, J.L. Hesler, H. Xu et al., A broadband quasi-optical THz detector using a zero bias Schottky diode // *IEEE Microwave and Wireless Components Lett.* **20**, p. 504 (2010).
17. A.J.M. Kreisler, Submillimeter wave applications of submicron Schottky diodes // *Proc. SPIE*, **666**, p. 51-63 (1986).
18. W. Knap, V. Kachorovskii, Y. Deng et al., Non-resonant detection of terahertz radiation in field effect transistors // *J. Appl. Phys*. **91**, p. 9346-9353 (2002).
19. W. Knap and M. Dyakonov, Field effect transistors for terahertz applications, in: *Handbook of Terahertz Technology for Imaging, Sensing and Communications*, D. Saeedkia (ed.). Woodhead Publishing, Oxford, Cambridge, Philadelphia, New Delhi, 2013, p. 121-155.
20. C. Sydlo, O. Cojocari, D. Schonner et al., Fast THz detectors based on InGaAs Schottky diodes // *Frequenz*, **62**, p. 107-110 (2008).
21. S.-P. Han, H. Ko, J.-W. Park et al., InGaAs Schottky barrier diode array detector for a real-time compact terahertz line scanner // *Opt. Express*, **21**, p. 25874-25882 (2013).

22. V. Yu. Kachorovskii, S. L. Rumyantsev, W. Knap, and M. Shur, Performance limits for field effect transistors as terahertz detectors // *Appl. Phys. Lett*. **102**, 223505 (2013).
23. E. Öjefors, A. Lisauskas, D. Glaab, H.G. Roskos, and U.R. Pfeiffer, Terahertz imaging detectors in CMOS Technology // *J. Infrared Milli Terahz Waves*, **30**, p. 1269-1280 (2009).
24. S. Boppel, A. Lisauskas, V. Krozer, and H.G. Roskos, Performance and performance variations of sub-1 THz detectors fabricated with 0.15 µm CMOS foundry process // *Electr. Lett*. **47**, p. 661-662 (2011).
25. S.M. Sze and K.K. Ng, *Physics of Semiconductor Devices*, 3rd ed. Wiley-Interscience, 2006.
26. Y. Tsividis and C. McAndrew, *Operation and Modeling of the MOS Transistor*. Oxford University Press, 2011.
27. A.M. Cowley and H.O. Sorensen, Quantitative comparison of solid-state microwave detectors // *IEEE Trans. Microwave Theory and Techniq.* **14**, p. 588 (1966).
28. S. Preu, S. Kim, R. Verma, P. G. Burke, M.S. Sherwin, and A.C. Gossard, An improved model for non-resonant terahertz detection in field-effect transistors // *J. Appl. Phys*. **111**, 024502 (2012).
29. C.A. Balanis, *Antenna Theory Analysis and Design*, 3d Edition, Wiley, New Jersey, 2005.
30. J.L. Volakis (ed.), *Antenna Engineering Handbook*, 4th ed. New York, McGraw-Hill, 2007.
31. R. Tauk, F. Teppe, S. Boubanga et al., Plasma wave detection of terahertz radiation by silicon field effects transistoprs: Responsivity and noise equivalent power // *Appl. Phys. Lett*. **89**, 253511 (2006).
32. M.S. Shur and P. Maki (eds.), Advanced high speed devices, in: *Selected Topics in Electronics and Systems*, Vol. 51, World Scientific, Singapore, 2009, p. 1-187.
33. E. Ojefors, N. Baktash, Y. Zhao, R. Al Hadi, H. Sherry, and U. Pfeifer, Terahertz imaging detectors in a 65-nm CMOS SOI technology // *IEEE Europ. Solid-State Circuits Conf.*, Seville, Spain, September, 2010, p. 486-489.
34. U.R. Pfeifer, and E. Ojefors, A 600-GHz CMOS focal-plane array for terahertz imaging applications // *Proc. Europ. Solid-State Circuits Conf.*, 2008, p. 110-113.
35. A. Pleteršek, and J. Trontelj, A self-mixing NMOS channel-detector optimized for mm-wave and THZ signals // *J. Infrared Milli Terahz Waves*, **33**, p. 615-626 (2012).
36. F. Schuster, D. Coquillat, H. Videlier et al., Broadband terahertz imaging with highly sensitive silicon CMOS detectors // *Opt. Express*, **19**, p. 7827-7832 (2011).
37. R. Al Hadi, H. Sherry, J. Grzyb et al., A broadband 0.6 to 1 THz CMOS imaging detector with an integrated lens // *Microwave Symposium Digest (MTT), 2011 IEEE MTT-S Intern.*, Baltimore, MD, June 5-10, 2011, p. 1-4.
38. H. Sherry, R. Al Hadi, J. Grzyb, E. Ojefors, A. Cathelin, A. Kaiser, and U. R. Pfeifer, Lens-integrated imaging arrays in 65 nm CMOS technologies // *Radio Freq. Integrated Circuits Symposium (RFIC)*, 2011, IEEE, June 5 – 7, 2011, Baltimore, MD, p. 365-368.
39. F. Sizov, A. Golenkov, D. But, N. Sakhno, and V. Reva, Sub-THz radiation room temperature sensitivity of long-channel silicon field effect transistors // *Opto-Electr. Rev*. **20**, p. 194-199 (2012).
40. E.R. Brown, A.C. Young, J.E. Bjarnason, H. Kazemi, J. Zimmerman, and A.C. Gossard, Millimeter and sub-millimeter wave performance of an ErAs:InAlGaAs Schottky diode coupled to a single-turn square spiral // *Int. J. High Speed Electronics and System*, **17**, p. 383-394 (2007).
41. A. Semenov, O. Cojocari, H.-W. Hubers, F. Song, A. Klushin, and A.-S. Muller, Application of zero-bias quasi-optical Schottky-diode detectors for monitoring short-pulse and weak terahertz Radiation // *IEEE Electr. Device Lett*. **31**, p. 674-676 (2010).
42. A.C. Young, J.D. Zimmerman, E.R. Brown, and A.C. Gossard, High sensitivity in semimetal-semiconductor microwave rectifiers // *Appl. Phys. Lett.* **87**, 163506 (2005).
43. V.I. Shashkin, Yu.A. Drjagin, V.R. Zakamov, S.V. Krivov, L.M. Kukin & A.V. Murel, and Yu.I. Chechenin, Millimeter-wave detectors based on antenna-coupled low-barrier Schottky diodes // *Int. J. Infrared Milli Waves*, **28**, p. 945-952 (2007).
44. V. Kubarev, G.M. Kazakevitch, Y. Uk Jeong, and B.Ch. Lee, Quasi-optical highly sensitive Schottky-barrier detector for a wide-band FIR FEL // *Nuclear Instr. Methods Phys. Research*, **A 507**, p. 523-526 (2003).
45. R. Han, Y. Zhang, Y. Kim, D. Y. Kim, H. Shichijo, E. Afshari, and O. Kenneth, "80 GHz and 860 GHz image sensors using schottky-barrier diodes in 0.13 µm digital CMOS // *2012 IEEE Intern. Solid-State Circuits Conf. Digest*, p. 254-256 (2012).
46. P. Chahal, F. Morris, and G. Frazier, Zero bias resonant tunnel Schottky contact diode for wide-band direct detection // *IEEE Electr. Device Lett.* **26**, p. 894-896 (2005).
47. J.D. Sun, Y.F. Sun, D.M. Wu, Y. Cai, H. Qin, and B.S. Zhang, High-responsivity, low-noise, room-temperature, self-mixing terahertz detector realized using floating antennas on a GaN-based field-effect transistor // *Appl. Phys. Lett*. **100**, 013506 (2012).
48. S. Boppel, M. Ragauskas, A. Hajo et al., Terahertz edge detectionwithantenna-coupled field-effect transistors in 0.25 µm AlGaN/GaN technology // *39-th Int. Conf. IR, Mm and THz Waves*, September 14-19, 2014, Tuscon, AZ.

49. P. Sangare, G. Ducournau, B. Grimbert et al., Experimental demonstration of direct terahertz detection at room-temperature in AlGaN/GaN asymmetric nanochannels // *J. Appl. Phys.* **113**, 034305 (2013).
50. A.G. Golenkov, K.S. Zhuravlev, J.V. Gumenjuk-Sichevska, I.O. Lysiuk, F.F. Sizov, Sub-THz nonresonant detection in AlGaN/GaN hetero-junction FETs // *Semiconductor Physics, Quantum Electronics & Optoelectronics,* **18**, p. 40-45 (2015).
51. D.M. Yermolaev, K.M. Marem'yanin, D.V. Fateev et al., Terahertz detection in a slit-grating-gate field-effect-transistor structure // *Solid-State Electron*. **86**, p. 64-67 (2013).
52. F. Sizov, V. Reva, A. Golenkov, V. Zabudsky, Uncooled detector challenges for THz/sub-THz arrays imaging // *J. Infrared Milli Terahz Waves*, **32**, p. 1192-1206 (2011).
53. A. Golenkov, F. Sizov, Terahertz FET direct detection rectifying detectors // *Proc. Mediterranean Microwave Symposium,* Lecce, Italy, November 30 – December 2, 2015, p. 204-207.